

Magnetic order and transport in the heavy-fermion system CeCu_{6-x}Au_x

H. v. Löhneysen¹, A. Neubert¹, A. Schröder¹, O. Stockert¹, U. Tutsch¹, M. Loewenhaupt², A. Rosch³, and P. Wölfle³

¹ Physikalisches Institut, Universität Karlsruhe, D-76128 Karlsruhe, Germany

² Institut für Angewandte Physik, Technische Universität Dresden, D-01062 Dresden, Germany

³ Institut für Theorie der Kondensierten Materie, Universität Karlsruhe, D-76128 Karlsruhe, Germany

Abstract. We report on extensive elastic neutron scattering to determine the wave vector of the magnetic order in CeCu_{6-x}Au_x single crystals for $x > 0.1$. For all values of x investigated (0.2, 0.3, 0.5, 1.0) we find long-range incommensurate antiferromagnetic order with an ordering vector $\mathbf{Q} \approx (0.625 \ 0 \ 0.275)$ for $x = 0.2$, nearly unchanged for $x = 0.3$, and $\mathbf{Q} \approx (0.59 \ 0 \ 0)$ for $x = 0.5$, staying roughly the same for $x = 1.0$. In addition, short-range correlations are observed at $x = 0.2$, reminiscent of those found previously for $x = 0.1$. The ordered magnetic moment is found to increase rapidly for small x , and more slowly for the larger x values. The increase of the specific-heat anomaly at the ordering temperature with x is in qualitative accord with this behavior. Finally, data of the electrical resistivity for current flow along the three crystallographic directions are presented, showing a clear signature of the magnetic order. A theoretical interpretation of the interplay of magnetic order and transport in terms of (i) the partial suppression of the Kondo effect by the staggered magnetization and (ii) the anisotropic band structure induced by the staggered field is shown to account well for the data, provided the ordering vector \mathbf{Q} is close to $2k_F$, where k_F is a typical Fermi momentum.

PACS. 75.30.Mb Valence fluctuation, Kondo lattice, and heavy-fermion phenomena – 75.25.+z Spin arrangements in magnetically ordered materials – 72.15.Eb Electrical and thermal conduction in crystalline metals and alloys

1 Introduction

Heavy-fermion systems exhibit a fascinating interplay of magnetically ordered and non-magnetic groundstates and - in some systems - superconductivity [1]. It has been known for a decade that the heavy-fermion compound CeCu₆ which does not show magnetic order down to temperatures T of at least 5 mK [2,3] exhibits long-range antiferromagnetic order when alloyed with Au or Ag [4,5]. From the beginning, this has been explained [6] as arising from the interplay between onsite Kondo screening of the Ce magnetic moments in a crystal-field split $^2F_{5/2}$ doublet groundstate [7] and the RKKY interaction between Ce moments. The latter is favored by a weakening of the Kondo screening with increasing of the interatomic spacing upon alloying with Au. Indeed, the magnetic order can be suppressed in CeCu_{6-x}Au_x and a nonmagnetic groundstate is recovered upon application of a sufficiently high hydrostatic pressure [6,8]. The Kondo temperature T_K as estimated from the specific heat in large magnetic fields $B = 6$ T applied along the easy direction, decreases monotonically from $T_K = 6.2$ K ($x = 0$) to 4.6 K ($x = 0.5$) [9,10]. In line with this T_K decrease, the onsite fluctuation rate as measured with inelastic neutron scattering $\Gamma(T \rightarrow 0)$ which is attributed to the Kondo effect, is smaller by a

factor of ~ 2 in CeCu_{5.5}Au_{0.5} than in pure CeCu₆ [7]. Between $x = 0.1$ and 1, the Néel temperature T_N rises from 0 to 2.3 K and decreases sharply beyond $x = 1$. For $x \leq 1$ Au occupies exclusively the Cu(2) position in the orthorhombic CeCu₆ structure (Pnma) [13]. The change of dT_N/dx at $x = 1$ coincides with a subtle change within the orthorhombic structure: For $x < 1$ the lattice parameters a and c increase while b decreases with growing Au content, whereas for $x > 1$ all three lattice parameters a, b and c increase. (We neglect the small monoclinic distortion ($\approx 1.5^\circ$) of CeCu₆ occurring below $T_S \approx 200$ K [16]. This structural transition vanishes quickly with x , e.g. $T_S \approx 70$ K for $x = 0.1$ [17].) Long-range antiferromagnetic order was previously directly observed for $x = 0.5$, with incommensurate reflections along the a^* axis (we use the orthorhombic notation throughout) indicating a magnetic ordering wave vector $\mathbf{Q} = (0.59 \ 0 \ 0)$ [11]. At the critical concentration $x_c \approx 0.1$ for the appearance of long-range antiferromagnetic order, pronounced deviations from Fermi-liquid behavior are observed in the thermodynamic properties, i.e. specific heat and magnetization, and in the electrical resistivity [12,13]. The critical fluctuations associated with this quantum critical point have recently been identified [14,15].

In this paper, we present a comprehensive study of the long-range antiferromagnetism in $\text{CeCu}_{6-x}\text{Au}_x$. We will use elastic neutron scattering to characterize the magnetic ordering wave vector for several concentrations $x = 0.2, 0.3, 0.5$ and 1.0 . The rough estimate of the ordered magnetic moment will be compared to that inferred from the specific-heat anomaly. Electrical resistivity measurements along different directions reveal clear features attributed to the magnetic order and represent an independent source of information on the magnetic structure below T_N . We consider a phenomenological theory of the transport of heavy quasiparticles in a disordered lattice, which accounts well for the observed behavior. In fact, the results allow to confirm the direction of the ordering \mathbf{Q} vector. In addition they appear to indicate that the \mathbf{Q} vector is not too far from $2k_F$, where k_F is a typical Fermi momentum.

2 Experimental

All samples of this study were single crystals grown in a W crucible with the Czochralski technique. The neutron scattering experiments were performed at the Institut Laue-Langevin Grenoble, instrument IN 14 (for $x = 0.2$) and the Hahn-Meitner-Institut Berlin, instruments E 4 and V 2 ($x = 0.3, x = 1$). The previous results for $x = 0.5$ (as well as preliminary results for $x = 1$) were obtained at NIST, instrument B 9 [11]. The quasi-adiabatic heat-pulse technique was used for the measurement of the specific heat. The electrical resistivity $\rho(T)$ was measured on small rectangularly shaped bars cut from the same crystals as used for the neutron scattering. The standard four-probe technique was applied. Because of the small sample size, the absolute ρ values are accurate only within 20%.

3 Results

3.1 Neutron scattering

Although the present paper focuses on the magnetically ordered $\text{CeCu}_{6-x}\text{Au}_x$ alloys, we should mention at the outset that an important issue is to identify the nature of the fluctuations responsible for the nonmagnetic to magnetic transition at the critical concentration $x_c = 0.1$. We recently identified two-dimensional short-range fluctuations in the dynamical magnetic susceptibility for $x = 0.1$ from the observation of rod-like structures in the reciprocal ac plane [14] (cf. Fig. 2). These dynamic correlations evolve for $x = 0.2$ into short-range and long-range ordering peaks, both are located along these rods. Fig. 1 shows results of elastic scans across magnetic Bragg reflections taken at temperatures well below the ordering temperature. For $x = 0.2$ we find the above mentioned short-range magnetic order along the a^* axis with a wave vector $\mathbf{Q} = (0.79\ 0\ 0)$ (Fig. 1a). From the linewidth of the peaks, $\Delta q = 0.06$ r.l.u. (HWHM) in a^* , we deduce a correlation length of about 2.7 unit cells in the a direction which is somewhat

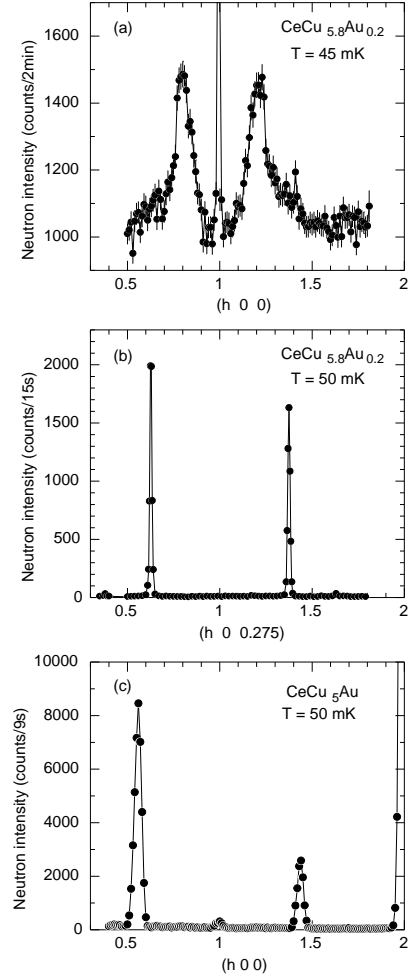


Fig. 1. a) and b): Elastic scans in $\text{CeCu}_{5.8}\text{Au}_{0.2}$ along $(h\ 0\ 0)$ and $(h\ 0\ 0.275)$ at temperatures $T \leq 50$ mK well below $T_N = 2.5$ K on IN 14 with a neutron energy $E = 2.7$ meV. The scans along the a^* axis reveal broad quasi-elastic structures indicating short-range correlations, while resolution-limited peaks are found at $(0.625\ 0\ 0.275)$ and equivalent positions. c): Elastic scan along $(h\ 0\ 0)$ in CeCu_5Au at $T = 50$ mK ($T_N = 2.3$ K) on E4 ($E = 14$ meV) showing resolution-limited peaks with $\mathbf{Q} = (0.56\ 0\ 0)$.

smaller than the results previously reported [18] (there a factor of $1/(2\pi)$ was omitted). This short-range order feature along the a^* axis was not observed for the $x = 0.3$ alloy probably due to large background compared to the expected magnetic intensity.

In addition, we observe resolution-limited reflections for $x = 0.2$ in the a^*c^* plane (Fig. 1b), indicating long-range magnetic order at $\mathbf{Q} = (0.625\ 0\ 0.275)$. Only minor changes in the positions of the magnetic peaks are found for $x = 0.3$ with $\mathbf{Q} = (0.62\ 0\ 0.253)$. In contrast, upon further Au doping for $x = 0.5$ the magnetic order no longer appears off the a^* axis, but incommensurate order is observed along a^* with $\mathbf{Q} = (0.59\ 0\ 0)$ [11] which is then roughly constant up to $x = 1$ ($\mathbf{Q} = (0.56\ 0\ 0)$). Since these experiments on $x = 0.5$ and 1 were performed long before

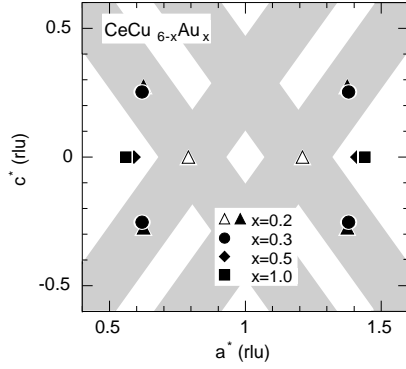


Fig. 2. Position of the magnetic Bragg peaks ($x = 0.2 - 1.0$) in the reciprocal ac plane in $\text{CeCu}_{6-x}\text{Au}_x$ (data for $x = 0.5$ taken from [11]). The open symbols for $x = 0.2$ represent the short-range ordering peaks and the stripes indicate the dynamic correlations found for $x = 0.1$ [14].

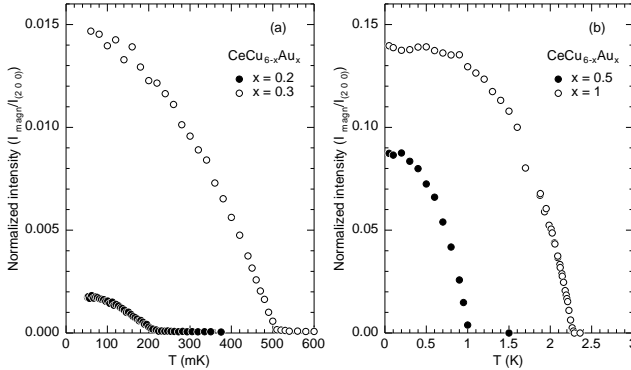


Fig. 3. Temperature dependence of the intensity of corresponding Bragg peaks normalized to the $(2\ 0\ 0)$ nuclear reflection for $x = 0.2$ ($\mathbf{Q} = (0.625\ 0\ 0.275)$) and $x = 0.3$ ($\mathbf{Q} = (0.62\ 0\ 0.253)$) in Fig. a and for $x = 0.5$ ($\mathbf{Q} = (0.59\ 0\ 0)$) and $x = 1.0$ ($\mathbf{Q} = (0.56\ 0\ 0)$) in Fig. b. The intensity is proportional to the square of the staggered magnetization $M_{\mathbf{Q}}(T)$.

the present ones on $x = 0.2$ and 0.3 , we did not take scans off the a^* axis and therefore cannot exclude some intensity at the positions out in the a^*c^* plane. On the other hand, powder measurements for $x = 0.5$ [16] do suggest that we did not miss an appreciable amount of magnetic intensity in our investigations on the single crystals. Fig. 2 summarizes the results obtained on the different $\text{CeCu}_{6-x}\text{Au}_x$ single crystals. The rod-like feature in $S(q, \omega = 0.1\text{ meV})$ of the alloy at the critical concentration $x_c = 0.1$ and the positions of the magnetic Bragg peaks are displayed in the reciprocal ac plane.

Fig. 3 shows the intensity of selected magnetic Bragg peaks as a function of temperature, one for each of the four investigated concentrations $x = 0.2, 0.3, 0.5$ and 1.0 . The peak intensity as normalized to the adjacent nuclear reflection, $(2\ 0\ 0)$, is seen to increase by a factor of 9 between $x = 0.2$ and 0.3 , while it increases more slowly between $x = 0.5$ and 1.0 . It should be mentioned that the intensity of the $(2\ 0\ 0)$ nuclear peak depends somewhat

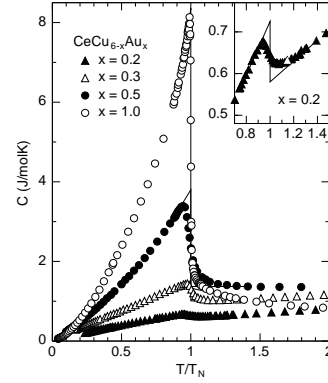


Fig. 4. Specific heat for $x = 0.2, 0.3, 0.5, 1.0$ as a function of T/T_N . The lines correspond to a mean-field transition with the same entropy contribution. The inset displays the specific heat for $x = 0.2$.

on the atomic positions inside the unit cell and is affected by extinction since $(2\ 0\ 0)$ is a strong peak. Therefore the normalized intensity of the magnetic peaks is only a rough measure of the size of the ordered magnetic moment. Because of the change of the magnetic structure and also of the scattering geometries between $x = 0.3$ and 0.5 , the intensities of Figs. 3a and 3b cannot be compared directly. Assuming a sinusoidal modulation of the moments aligned along c we estimate an ordered magnetic moment μ of $0.1 \dots 0.15 \mu_B/\text{Ce}$ atom for $x = 0.2$. Under the same assumptions the ordered moment for $x = 0.3$ is a factor of 3 larger. For $x = 0.5$ the estimate of $\mu \approx 1 \mu_B/\text{Ce}$ atom had been given previously [11]. Fig. 3b shows that this value increases only by small percentage for $x = 1.0$. These numbers should be compared to $2.54 \mu_B$ for free Ce^{3+} moments. For CeCu_6 the magnetization measured along the c axis yields a magnetic moment of $1.5 \mu_B/\text{Ce}$ atom in an applied field of 40 T [19]. Theoretically, the ordered magnetic moment in a weakly interacting itinerant-electron model should depend on the Néel temperatures as $\mu \propto T_N^{3/4}$ [20] which gives a slower increase of the moment than experimentally observed.

Although the ordering wave vector for $x = 0.5$ and 1.0 as taken from $(h\ 0\ 0)$ scans is not changing very much, the intensity of several reflections in the a^*b^* plane off the a^* axis, not observed for $x = 0.5$ is clearly not compatible with a simple sine-modulated structure. For $x = 1.0$ a complex magnetic (B, T) phase diagram has been observed, with the magnetic structure found in zero applied magnetic field B giving way to a different structure in $B > 0$ via a first-order phase transition [21]. Neutron scattering studies in magnetic fields are underway to examine the magnetic structure in these phases.

3.2 Specific-heat anomaly at the ordering temperature

The specific heat of the $\text{CeCu}_{6-x}\text{Au}_x$ single crystals has been measured as reported in detail elsewhere [9,10,21]. Here we focus on the anomaly at T_N . Fig. 4 shows C plotted vs. reduced temperature T/T_N . As noted before [9] the

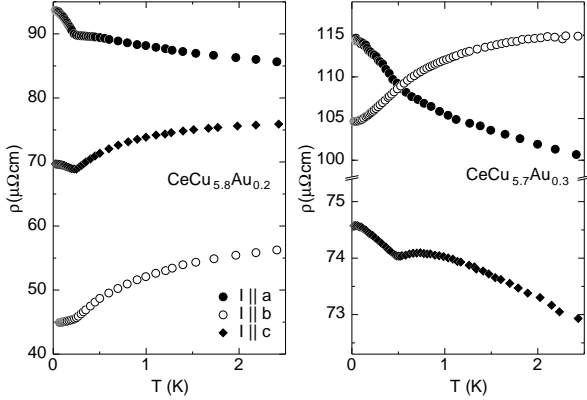


Fig. 5. Resistivity of $\text{CeCu}_{5.8}\text{Au}_{0.2}$ and $\text{CeCu}_{5.7}\text{Au}_{0.3}$ along the three crystallographic axes. Along the a and c direction a sharp rise of the resistivity is observed at the Néel temperature ($T_N \approx 0.25$ K for $x = 0.2$ and $T_N \approx 0.51$ K for $x = 0.3$).

specific heat looks almost mean-field like for $x = 0.3$ and 0.5 . On the other hand it is more rounded for $x = 0.2$ and more peaked for $x = 1.0$. There is a considerable contribution arising from short-range ordering above T_N as evidenced from the tail of the anomaly. The strong increase of the specific-heat anomaly with x qualitatively underscores the increase of the ordered moment already inferred from the neutron scattering. A more detailed analysis must await a microscopic model of the alloying effect in $\text{CeCu}_{6-x}\text{Au}_x$ (see also section 4). In a crude analysis, we replace the observed anomaly at T_N by a mean-field discontinuity ΔC under the usual entropy - conserving construction (cf. thin lines in Fig. 4). For an ordered spin moment of $s = \frac{1}{2}$ one expects $\Delta C_{MF} = 1.5R$ [22]. We find the following values $r = \Delta C / \Delta C_{MF}$ for $x = 0.2, 0.3, 0.5$ and 1 : $r = 0.016, 0.04, 0.2,$ and 0.55 , respectively. One should keep in mind that even for $x = 1$ a considerable Kondo effect is operative indicated by a sizable $\gamma = 0.64 \text{ J/molK}^2$ at 0.1 K in zero magnetic field [21].

3.3 Resistivity

Fig. 5 gives an overview over the T dependence of the electrical resistivity ρ for $x = 0.2$ and 0.3 . For both concentrations, $\rho(T)$ shows a kink at the Néel temperature T_N and increases below T_N for current direction I parallel to a and c while $\rho_b(T)$ for $I \parallel b$ continues to decrease towards lower temperatures. For both concentrations $\rho_a(T)$ has a negative temperature coefficient throughout the T range investigated, and exhibits the largest magnitude compared to ρ_b and ρ_c below T_N .

These findings suggest that below the Néel temperature quasiparticle scattering properties are changed. This can happen in several different ways as will be discussed in section 4. We mention that resistivity data for $x = 0.15$ where only ρ_a and ρ_b were measured [23] fit nicely into this picture, i.e. an increase of $\rho_a(T)$ below T_N and a decrease of $\rho_b(T)$ is observed.

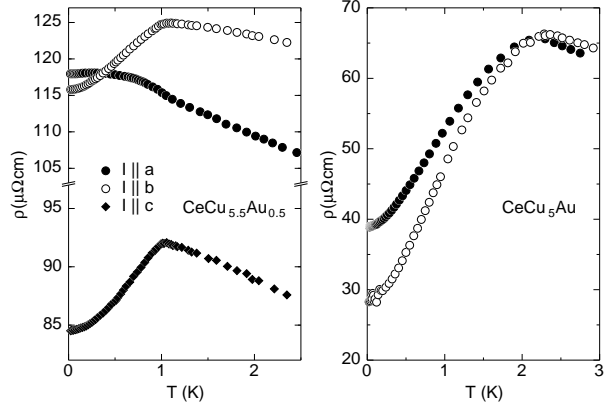


Fig. 6. Resistivity of $\text{CeCu}_{5.5}\text{Au}_{0.5}$ and CeCu_5Au_1 . Along the a -axis a sharp rise of the resistivity is observed at the Néel temperature for $x = 0.5$ ($T_N \approx 1.0$ K). For $x = 1$ ($T_N \approx 2.3$ K) the resistivity decreases with temperature both in a and b direction, however the decrease along a seems to be smaller.

Fig. 6 shows $\rho(T)$ for $x = 0.5$ and 1 . While for $x = 0.5$ $\rho_a(T)$ again exhibits a (weak) kink at T_N and increases faster towards low T , ρ_b and ρ_c reveal a rather sharp maximum at T_N . Again, these features can be explained by referring to the magnetic structure. For this concentration, the magnetic ordering vector lies on the a^* axis hence only this direction shows an increase of $\rho(T)$ below T_N .

For $x = 1$ (Fig. 6b) we observe a maximum of $\rho(T)$ at T_N both for $I \parallel a$ and $I \parallel b$. However, the decrease of $\rho_a(T)$ below T_N is slower than that of $\rho_b(T)$. It is important to note that even for $x = 1$, a very large residual linear specific-heat coefficient $\gamma = 0.64 \text{ J/molK}^2$ is observed in the magnetically ordered state [21].

As a final result, we plot in Fig. 7 the residual resistivity ρ_0 for the three current directions as a function of Au concentration x . As already apparent from the data of Fig. 5 and 6, $\rho_{0,a}$ is largest throughout the concentration range. The maximum of $\rho_{0,a}$ at $x \approx 0.5$ reflects the large structural disorder although the system is magnetically homogeneous as evidenced from the resolution-limited Bragg peaks.

4 Interplay of magnetic order and transport

As a theoretical model for $\text{CeCu}_{6-x}\text{Au}_x$ we envisage a conduction band of heavy quasiparticles generated by the Kondo effect at the Ce ions. Their effective mass m and Fermi energy ϵ_F is controlled by the Kondo temperature T_K , i.e. $m \sim (T_F/T_K)m_{\text{band}}$, $\epsilon_F \sim T_K$, there T_F and m_{band} are the Fermi temperature and bare mass of the weakly interacting conduction electrons. The substitution of Au for Ce in CeCu_6 is known to take place at a special Cu site next to each of the four Ce atoms in the unit cell (see section 1). The overall effect of alloying on the heavy fermion liquid is to lower the Kondo temperature mildly (up to a factor ~ 2 for $x = 1$), as inferred from

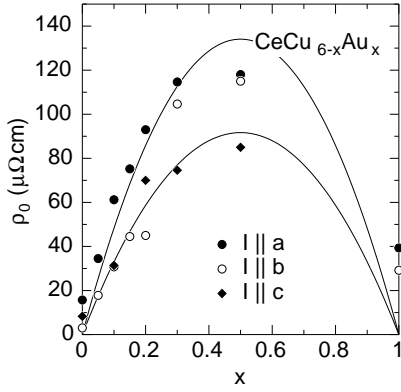


Fig. 7. Residual resistivity along the a , b and c axis as a function of doping x . The solid lines denote the Nordheim relation $\rho \propto x(1-x)$.

the γ coefficient of the specific heat and the quasi-elastic linewidth ($\sim T_K$) in neutron scattering. It is not known at present, whether this must be interpreted as a lowering of the characteristic energy of the coherent state of the Kondo lattice forming at low temperatures, caused by the lattice distortions and the associated (probable) lowering of the conduction electron density of states at the Fermi energy and the weakening of the f-d hybridization, or as a local lowering of the Kondo temperature at those Ce ions next to a Au atom. In any case it will be useful to distinguish the single-ion regime above the so-called coherence temperature T_0 , defined by the maximum in the resistivity as a function of temperature, from the lattice-coherent state below T_0 .

The most prominent consequence of coherence is that for a regular lattice of Kondo ions, i.e. in the stoichiometric compounds CeCu_6 and CeCu_5Au , the resistivity should tend to zero in the limit $T \rightarrow 0$. This is seen in Fig. 7 where the residual resistivity is plotted versus Au concentration x . The fact that for $x = 1$ the residual resistivity ρ_0 is not quite zero, but assumes minimum values of $30\text{-}40\mu\Omega\text{cm}$, is likely due to remaining lattice defects. The data points are roughly consistent with the law $\rho_0 \sim x(1-x)$. The maximal values for ρ_0 are of the order of the unitarity limit, i.e. correspond to a mean free path of the order of the Fermi wavelength. This suggests that the Au impurities act as strong scatterers, probably because they change the Kondo state of the nearby Ce ion in a subtle way. We recall that the Kondo temperature in the doped systems is only a factor two or so smaller than that of CeCu_6 , so we have no indication for a drastic suppression of the Kondo effect by the Au impurities. Nonetheless, the additional potential scattering caused by the Au impurities may change the f-level occupation on the Ce ions sufficiently to induce a relevant deviation of the Kondo phase shift from the value $\pi/2$. In any case, it is reasonable to assume that the observed strong increase of ρ_0 with Au concentration is related to the Kondo effect in the Ce ions.

This suggests the following scenario: at any finite temperature not too far below T_K the magnetic moments at the Ce ions are not completely quenched by the Kondo

effect. The residual moments interact and may form an ordered magnetic state. Even in the fully developed magnetically ordered state at $T = 0$ the local magnetic field created by the ordered spin configuration may be sufficiently small such that a reduced Kondo effect remains. For a range of values of $T_K \gtrsim T_N$ the Kondo effect and magnetic order may thus coexist. An alternative scenario would be that of a spin density wave of the heavy quasiparticles. While the latter model may have difficulties to explain the rather large magnetic moments experimentally observed at $x = 0.5$ and $x = 1.0$, it can not be ruled out at present.

We consider now the effect of magnetic order on the resistivity. Within the first scenario the onset of magnetic order would be associated with a partial suppression of the Kondo effect by the local magnetic field generated by the ordered moments. The effect of a magnetic field H on the resistivity ρ_K of a single $S = 1/2$ Kondo ion at $T = 0$ can be exactly expressed in terms of the Kondo impurity magnetization M_K as [24]

$$\rho_K = \rho_K(0) \cos^2 \left(\frac{\pi M_K}{g\mu_B} \right) \quad (1)$$

We expect this relation to hold approximately at finite temperatures $T_0 \lesssim T \lesssim T_K$ as well. Taking the magnetization to be proportional to the ordered moment $M_{\mathbf{Q}}(T)$, we obtain the following estimate of a first effect of the magnetic order on the resistivity of the Kondo alloys in the single-ion regime

$$\rho(T, M_{\mathbf{Q}}(T)) = \rho(T, M_{\mathbf{Q}} = 0) \cos^2 \left(\frac{\alpha M_{\mathbf{Q}}}{g\mu_B} \right) \quad (2)$$

where α is a coefficient of order unity. This will tend to reduce all components of the resistivity tensor equally strongly. The initial (isotropic) decrease below T_N according to (2),

$$\frac{\delta\rho^{(1)}}{\rho_0} \approx -\frac{1}{2}\alpha^2 \left(\frac{M_{\mathbf{Q}}(T)}{g\mu_B} \right)^2, \quad (3)$$

is proportional to $M_{\mathbf{Q}}^2(T)$ and hence linear in $(T_N - T)$ near T_N . For the experimentally determined temperature dependence of $M_{\mathbf{Q}}(T)^2$ see Fig. 3.

Secondly, the periodically modulated static spin structure in the magnetically ordered state will give rise to a change in the conduction-electron band structure. This is independent of whether the magnetism is of an itinerant or a localized nature. Roughly speaking, the additional periodic structure will give rise to enhanced back-scattering for quasiparticles moving in the direction of the magnetic wave vector \mathbf{Q} , hence increasing the resistivity components along \mathbf{Q} . This is born out by the data of Fig. 5, which indeed show an increase of ρ along the a and c directions, in accordance with the direction of $\mathbf{Q} \approx (0.625 \ 0 \ 0.275)$ for $x = 0.2$ while ρ increases only in the a direction for $x = 0.5$ with $\mathbf{Q} \approx (0.59 \ 0 \ 0)$.

We will sketch a model calculation of this effect in the following. The static magnetization associated with the

magnetic order acts like an additional (spin-dependent) periodic potential, thus changing the band structure. As this change is small it can be calculated in degenerate perturbation theory. The band structure affects both the quasiparticle energy $\epsilon_{\mathbf{k}}$ and the transport relaxation time $\tau_{\mathbf{k}}$. For a quantitative theory of this effect a detailed knowledge of the band structure, the magnetic ordering, the interactions of the staggered moment with the electrons and the momentum dependence of $\tau_{\mathbf{k}}$ is necessary. The qualitative effect, however, can easily be calculated, e.g. for a spherical Fermi surface assuming isotropic scattering. The staggered magnetization $M_{\mathbf{Q}}(T)$ induces a spin-dependent periodic potential of wave vector \mathbf{Q} . It is now important to distinguish three different scenarios, depending on whether the ordering wave vector \mathbf{Q} is larger, smaller or of the order of the size of the Fermi sphere with radius k_F . For $Q \gg 2k_F$ the resistivity is practically not affected by the short-range periodic potential. For $Q < 2k_F$ belts of band-gaps are opened at the Fermi surface for $\epsilon_{\mathbf{k}} \approx \epsilon_{\mathbf{k} \pm \mathbf{Q}}$. The magnitude of those energy-gaps is proportional to $M_{\mathbf{Q}}(T)$.

The model is described by the following Hamiltonian

$$H_0 = \sum_{\mathbf{k}, \sigma} \epsilon_{\mathbf{k}} c_{\mathbf{k}\sigma}^\dagger c_{\mathbf{k}\sigma} + \Delta \sum_{\mathbf{k}} \left(c_{\mathbf{Q}/2+\mathbf{k}\downarrow}^\dagger c_{-\mathbf{Q}/2+\mathbf{k}\uparrow} + h.c. \right). \quad (4)$$

\mathbf{Q} is the ordering wave vector, $\epsilon_{\mathbf{k}}$ is the energy spectrum in the absence of the magnetic order. We have assumed a sinusoidal variation of the magnetization directed along the spin quantization axis of the electrons. Δ measures the strength of the effective potential and is proportional to the staggered magnetization $M_{\mathbf{Q}}(T)$ measured in neutron scattering. The energy eigenvalues of H_0 are given by ($\hbar = 1$)

$$E_{\mathbf{k}}^\pm = \frac{\epsilon_{\mathbf{Q}/2+\mathbf{k}} + \epsilon_{\mathbf{Q}/2-\mathbf{k}}}{2} \pm \sqrt{\left(\frac{\epsilon_{\mathbf{Q}/2+\mathbf{k}} - \epsilon_{\mathbf{Q}/2-\mathbf{k}}}{2} \right)^2 + \Delta^2} \\ = \Delta\epsilon_0 + k_{\parallel}^2/2m + \mathbf{k}_{\perp}^2/2m \pm \sqrt{(v_0 k_{\parallel})^2 + \Delta^2} \quad (5)$$

We will use a quadratic band structure $\epsilon_{\mathbf{k}} = k^2/2m$ throughout the paper, as no information is available on the complicated band structure of CeCu₆. The qualitative conclusions drawn from this model will nonetheless be correct, although we expect that quantitative changes will result from a realistic band structure. As we are considering a heavy-fermion system we expect m to be very large, with the Fermi energy $k_F^2/2m \sim T_K$ (~ 6 K for CeCu₆) taking a rather low value. The variables k_{\parallel} and \mathbf{k}_{\perp} are the components of the momentum parallel and perpendicular to \mathbf{Q} and k_{\parallel} is confined to the first (magnetic) Brillouin zone, $-Q/2 \leq k_{\parallel} \leq Q/2$. $v_0 = Q/2m$ is the velocity at $\mathbf{Q}/2$ parallel to \mathbf{Q} and $\Delta\epsilon_0 = (\mathbf{Q}/2)^2/2m - \mu$ is negative (positive) for $\mathbf{Q} < 2k_F$ ($\mathbf{Q} > 2k_F$), where $\mu \equiv k_F^2/2m$ is the chemical potential.

In the following we will investigate within a simple Boltzmann transport picture the interplay of impurity scattering and the change of the band structure due to the

static magnetic order. We will not consider inelastic processes like the scattering of electrons from magnetic fluctuations, which are probably negligible at some distance from the transition and at the low temperatures considered. The change of the band structure affects both the scattering rate of the electrons and the velocities of the fermions at the Fermi surface. The change of the chemical potential due to Δ can be neglected as it is proportional to $(\Delta/\epsilon_F)^2 \ln[\epsilon_F/(\Delta + \Delta\epsilon_0)]$ and therefore small compared to the other effects discussed below.

The transport scattering rate $1/\tau_{\mathbf{k}}$ near the Fermi surface due to impurity scattering is given by

$$\frac{1}{\tau_{\mathbf{k}'}} = \sum_{i=\pm} \int d^2\mathbf{k}_{\perp} dk_{\parallel} \delta(E_{\mathbf{k}}^i) (1 - \cos \phi_{kk'}) W_{kk'} \quad (6)$$

where $\phi_{kk'}$ is the angle between $\mathbf{v}_{\mathbf{k}}^\pm = dE_{\mathbf{k}}^\pm/d\mathbf{k}$ and $\mathbf{v}_{\mathbf{k}'}^\pm$. For simplicity we consider only s-wave scattering ($W_{kk'} = \text{const.}$), for which the cosine drops out due to $\cos \phi + \cos(\pi - \phi) = 0$. The integration on k_{\parallel} yields a constant value for $0 \leq k_{\parallel} \leq k_{\parallel}^{\text{max}}$ where $k_{\parallel}^{\text{max}} = Q/2$ for $i = -$ and $k_{\parallel}^{\text{max}} < Q/2$ for $i = +$, in the case that $Q < 2k_F$. (In the opposite case $Q > 2k_F$ the contributions stem from $k_{\parallel}^{\text{max}} \leq k_{\parallel} \leq Q/2$ and $i = -$ and $E_{\mathbf{k}}^+$ is not occupied.) From the condition $E_{\mathbf{k}}^\pm(\mathbf{k}_{\perp} = 0, k_{\parallel}) = 0$ we obtain $k_{\parallel}^{\text{max}} = \sqrt{k_F^2 + (Q/2)^2 - 2\sqrt{k_F^2(Q/2)^2 + m^2\Delta^2}} \approx \sqrt{(k_F - (Q/2))^2 - m^2\Delta^2/(k_F(Q/2))}$ with $E_{\mathbf{k}}^+(0, k_{\parallel}^{\text{max}}) = 0$ for $Q < 2k_F$ and $E_{\mathbf{k}}^-(0, k_{\parallel}^{\text{max}}) = 0$ for $Q > 2k_F$. For $Q > 2k_F$ only $E_{\mathbf{k}}^-$ gives a contribution to the scattering rate, $1/\tau_{\mathbf{k}} \propto Q/2 - k_{\parallel}^{\text{max}}$. For $Q < 2k_F$ we obtain from the lower band always the same contribution $\propto Q/2$ while from the upper band one has to add a contribution $\propto k_{\parallel}^{\text{max}}$. Combining this we find that the relative change of the scattering rate due to the opening of a gap is given by

$$\delta \left(\frac{1}{\tau_{\mathbf{k}}} \right) / \left(\frac{1}{\tau_{\mathbf{k}}} \right) = \frac{1}{k_F} \left(\frac{Q}{2} - k_F \mp \text{Re} \sqrt{\left(\frac{Q}{2} - k_F \right)^2 - \frac{m^2\Delta^2}{k_F Q/2}} \right) \quad (7)$$

where the $+$ ($-$) is valid for $Q < 2k_F$ ($Q > 2k_F$). Re denotes the real part, taking into account that the band gives no contribution, if it is not occupied. For $Q < 2k_F$ the scattering rate is *reduced* by $1 - Q/(2k_F)$ for $\Delta < |\Delta\epsilon_0|$ and by $\Delta^2/(8\epsilon_F(Q/2)^2/(2m))Q/(2k_F - Q)$ for $\Delta > |\Delta\epsilon_0|$. For $Q > 2k_F$ the scattering rates are *increased* by the same amount. As the change of the scattering rate is approximately of the order of $(\Delta/\epsilon_F)^2(Q/(Q - 2k_F))$ large effects are expected only for $Q \approx 2k_F$.

The conductivity due to impurity scattering is given by

$$\sigma_{\alpha\beta} = -e^2 \sum_{i=\pm} \int v_{\alpha}^i v_{\beta}^i f'(E_{\mathbf{k}}^i) \tau_{\mathbf{k}} d^3\mathbf{k} / (2\pi)^3 \quad (8)$$

$$\approx e^2 \tau(\Delta) \sum_{i=\pm} \int \frac{\partial^2 E_{\mathbf{k}}^i}{\partial k_{\alpha} \partial k_{\beta}} f(E_{\mathbf{k}}^i) \quad (9)$$

where $\mathbf{v}^i = \partial E_{\mathbf{k}}^i / \partial \mathbf{k}$ is the velocity of the quasiparticles, $f(\epsilon_{\mathbf{k}})$ is the Fermi function and $\tau_{\mathbf{k}}$ the (elastic) transport scattering time of the quasiparticles.

Let us first consider the components of σ perpendicular to \mathbf{Q} , σ_{\perp} . Within the model considered, the perpendicular components of the inverse effective mass tensor $\partial^2 E_{\mathbf{k}}^i / \partial k_{\alpha} \partial k_{\beta} = 1/m$ are unchanged by the magnetic order. The conductivity is given by the Drude result $\sigma_{\perp} = e^2 n \tau / m$ with, however, the proper relaxation time τ changed by the gap according to Eq. (7). This yields a relative change of the resistivity ρ_{\perp} induced by the magnetic order, which is in leading order in Δ

$$\frac{\delta \rho_{\perp}^{(2)}}{\rho_0} = -\frac{1}{4} \frac{k_F^2}{Q(k_F - Q/2)} \left(\frac{\Delta}{\epsilon_F} \right)^2. \quad (10)$$

This estimate holds provided that $|k_F - Q/2| > m\Delta/k_F$. It is seen that the conductivity is increased (decreased) for $Q < 2k_F$ ($Q > 2k_F$) by an amount proportional to the squared amplitude of the magnetic order $M_{\mathbf{Q}}(T)$. Except for small $(k_F - Q/2)$ the effect is of order $(T_N/T_K)^2$ where T_N and T_K are the Néel and Kondo temperatures, respectively.

The conductivity component parallel to \mathbf{Q} is mainly affected by the change in the effective mass tensor

$$\frac{\partial E_{\mathbf{k}}^{\pm}}{\partial k_{\parallel}^2} = \frac{1}{m} \pm \frac{v_0^2 \Delta^2}{((v_0 k_{\parallel})^2 + \Delta^2)^{3/2}}. \quad (11)$$

Performing the integration on \mathbf{k}_{\perp} in (9) one finds

$$\Delta \sigma_{\parallel}^{(3)} = -e^2 \tau m v_0^2 \Delta^2 \int \frac{dk_{\parallel}}{(2\pi)^2} \frac{T \ln[(1 + e^{X_+}) / (1 + e^{X_-})]}{[(v_0 k_{\parallel})^2 + \Delta^2]^{3/2}} \quad (12)$$

where $X_{\pm} = -E^{\mp}(k_{\parallel}, \mathbf{k}_{\perp} = 0) / T$. For $Q \lesssim 2k_F$ ($\Delta \epsilon_0 \lesssim 0$) and $\Delta \ll |\Delta \epsilon_0|$ or else $\Delta \ll T$, one finds for the change in resistivity

$$\frac{\delta \rho_{\parallel}^{(3)}}{\rho_0} = \left(1 - \frac{3\pi v_0}{2 v_F \epsilon_F} \Delta f(\Delta \epsilon_0) \right)^{-1} \approx \frac{3\pi v_0}{2 v_F \epsilon_F} \Delta f(\Delta \epsilon_0). \quad (13)$$

This contribution has to be added to the one induced by the change in the relaxation rate, $\delta \rho_{\parallel}^{(2)} / \rho_0 = \delta \rho_{\perp}^{(2)} / \rho_0$ which was found to be quadratic in Δ , and hence is smaller.

On top of the contributions (10) and (13) we have to add the contribution found in (3), which is in principle comparable in magnitude to (10).

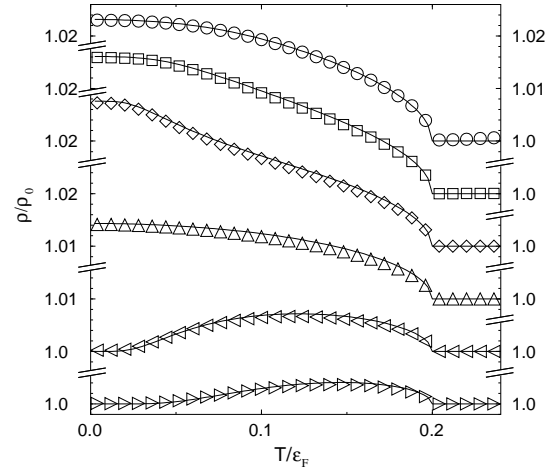


Fig. 8. Increase of the resistivity $\rho_{\parallel}^{(3)}$ due to band structure effects for the model described in Eqn. (4) for $T_N = 0.2\epsilon_F$. The gap $\Delta(T)$ is assumed to be proportional to $M_{\mathbf{Q}}(T)$ derived from Fig. 3: $\Delta(T)/\epsilon_F = 0.15(T_N/\epsilon_F)\sqrt{1 - (T/T_N)^2}$. The result is given for various ordering vectors from top to bottom: $Q/2 = 0.8k_F, 0.9k_F, 0.95k_F, k_F, 1.05k_F, 1.1k_F$. For clarity we have plotted the curves with a constant offset. The points are the result of a numerical evaluation of (9), the solid lines show our approximating formula (13).

The theoretical estimates derived above allow to interpret the data shown in Fig. 5 and 6 in a satisfactory way. For all Au concentrations shown, the resistivity increases below T_N with decreasing temperature relative to the (extrapolated) background only for those directions of current flow with a finite projection onto the ordering vector \mathbf{Q} (the effect being the larger, the larger the projection). This is in accordance with our result that only for those directions the dominant term linear in Δ , given by (13), contributes. It remains to explain the temperature dependence of this effect, which appears to be rather more linear than square root. However, although (13) appears to give a square-root dependence on $(T_N - T)$ due to the linearity in $\Delta \propto M_{\mathbf{Q}}(T)$, a numerical evaluation shows (Fig. 8) that for \mathbf{Q} sufficiently close to $2k_F$ and T_N not too small compared to ϵ_F the temperature dependence of the Fermi function $f(\Delta \epsilon_0)$ in the relevant temperature regime tends to straighten the square-root towards linear behavior over a wide range in temperature. This would indicate that for both $x = 0.2, 0.3$ and $x = 0.5, 1.0$, \mathbf{Q} is close to spanning the distance between sections of the Fermi surface with opposite Fermi velocities ($\mathbf{Q} \sim 1.8k_F - 2k_F$). A fit of the results for $\delta \rho_{\parallel}^{(3)}$ (13) to the data is not easy due to the unknown background and the additional isotropic contribution from $\rho^{(1)}$ and $\rho^{(2)}$. We find roughly for the ratio $\Delta/\epsilon_F \approx 0.1(T_N/T_K)(M_{\mathbf{Q}}(T)/M_{\mathbf{Q}}(0))$.

Let us now turn to the components of ρ perpendicular to \mathbf{Q} . In this case only the contributions $\delta \rho^{(1)}$ and $\delta \rho^{(2)}$ survive, which are both quadratic in $M_{\mathbf{Q}}(T)$. Of these, $\delta \rho^{(1)}$ is probably the dominant one, considering the small value of Δ/ϵ_F . Using the values of the low temperature staggered magnetization estimated from the neutron scat-

tering data, $M_{\mathbf{Q}}(0)/\mu_B \approx 0.1, 0.3, 1$ for $x = 0.2, 0.3$ and 1.0 we find a drop in resistivity from T_N to $T = 0$ of relative magnitude $\delta\rho^{(1)}(T = 0)/\rho(T_N) \sim 0.001, 0.01, 0.1$ taking $\alpha = 1$ and $g = 2\mu_{\text{sat}}/\mu_B \approx 2.8$ in (3). This compares well with the experimental data for which an additional drop of ρ_b towards lower temperatures, on top of the decrease caused by the formation of coherence, is not noticeable for $x = 0.2$ and 0.3 , whereas for $x = 0.5$ the relative change is roughly $\delta\rho/\rho \sim 0.1$. For the highest concentration $x = 1$, the predicted drop $\delta\rho^{(1)}/\rho \sim 0.15$ accounts for part of the total drop, the main part being due to coherence effects. For $x = 0.2$, the resistivity ρ_b is seen to rise for decreasing temperature with respect to an extrapolated background, probably due to admixtures from components parallel to \mathbf{Q} . Another possibility is that \mathbf{Q} may be slightly larger than $2k_F$ and $\rho^{(2)}$ taken from (10) is positive. However, this is difficult to decide as long as the band structure is unknown and the temperature dependence in the absence of magnetic order is not fully understood.

In a more general view, the resistivity data show clear signs of the existence of three characteristic temperatures, the Kondo temperature T_K (\sim Fermi energy of the heavy quasiparticles), the coherence temperature T_0 and the Néel temperature T_N . For temperatures above T_0 , the resistivity components show the negative temperature coefficient characteristic of the single-ion Kondo effect, whereas for T less than T_0 the temperature coefficient changes to positive, even though in the disordered samples (for $0 < x < 1$) the resistivity has a finite zero-temperature limit. Superposed on this background is an abruptly appearing change for $T < T_N$ caused by the growing magnetic order as discussed above. Here one has to keep in mind that the coherence temperature by definition can not be uniquely defined, as it is meant to characterize a smooth crossover rather than a phase transition. The positions of the maxima of ρ , which are significant for the onset of coherence, are seen to vary broadly for the different resistivity components, reflecting the complex band structure of the system. Nonetheless, the main features of the resistivity fit well into this picture. The data seem to indicate that for $x \geq 0.5$ the system is in the regime where $T_0 < T_N$, while for $x \leq 0.3$ we observe $T_0 \gtrsim T_N$. This may in part be responsible (beside the much smaller magnetization for $x \leq 0.3$ suppressing all quadratic effects) for the fact that the decrease of resistivity perpendicular to \mathbf{Q} is much larger for the higher Au concentrations.

5 Conclusions

The neutron-scattering data of the heavy-fermion alloy $\text{CeCu}_{6-x}\text{Au}_x$ reported here show that a complex magnetic structure appears at low temperatures. As discussed in previous publications, near the quantum-critical point at $x \approx 0.1$ two-dimensional fluctuations are found to dominate. In the magnetically ordered phase for $x > 0.1$, considered in this paper, incommensurate order emerges, characterized by an ordering wave vector in the a^*c^* plane for $x = 0.2$ and 0.3 , changing to a different wave vector

for $x = 0.5$ and $x = 1$. The appearance of magnetic order has a profound effect on the electrical-resistivity components. Broadly speaking, the resistivity tends to increase with staggered magnetization for current directions along the wave vector \mathbf{Q} , while it tends to decrease for all other directions, between $x = 0.3$ and $x = 0.5$. We have shown that a pronounced increase of the resistivity proportional to the staggered moment is indeed expected for current parallel to \mathbf{Q} . This effect is caused by the change in the band structure induced by the scattering of the heavy quasiparticles off the periodically varying magnetization. In addition we identified two contributions in the resistivity proportional to the staggered moment squared, the first one induced by the partial quenching of the Kondo effect through the staggered magnetic field and therefore negative, and the second one following from the change of the momentum relaxation rate, with positive (negative) sign for $Q > 2k_F$ ($Q < 2k_F$). We found indications that Q is close to $2k_F$, where k_F is a Fermi vector of the band structure in the direction of \mathbf{Q} .

In this scenario we obtain a satisfactory picture of the interplay of magnetic order and transport in $\text{CeCu}_{6-x}\text{Au}_x$ for $0.2 \leq x \leq 1$. A more detailed understanding requires knowledge of the electronic band structure of CeCu_6 , as well as a microscopic theory of the Kondo lattice and to the heavy fermion states, which is not yet available.

We wish to thank N. Pyka and S. Pujol from the Institut Laue-Langevin in Grenoble and E. Garcia-Matres, R. v. d. Kamp, S. Welzel and H. Schneider at the Hahn-Meitner-Institut in Berlin for their help on neutron scattering and G. Portisch and H. G. Schlager for preparing some of the crystals. We acknowledge the assistance of R. Häußler on some resistivity measurements. This work was supported by the Deutsche Forschungsgemeinschaft.

References

1. P. Fulde et al., *Solid State Phys.* **41**, 1 (1988); N. Grewe and F. Steglich, in: *Handbook on the Physics and Chemistry of Rare Earths*, vol 14, ed. by K. A. Gschneidner Jr. and L. Eyring (Amsterdam: Elsevier), p. 343
2. E. A. Schubert et al., *Phys. Rev. B* **51**, R 12892 (1995)
3. L. Pollack et al., *Phys. Rev. B* **52**, R 15707 (1995)
4. A. Germann et. al., *J. de Phys. (Paris) Colloq.* **49**, C8-75 (1988)
5. A. K. Gangopadhyay et al., *Phys. Rev. B* **38**, 2603 (1988)
6. A. Germann and H. v. Löhneysen, *Europhys. Lett.* **9**, 367 (1989)
7. B. Stroka et al., *Z. Physik B* **90**, 155 (1993)
8. B. Bogenberger and H. v. Löhneysen, *Phys. Rev. Lett.* **74**, 1016 (1995)
9. H. G. Schlager et al., *J. Low Temp. Phys.* **90**, 181 (1993)
10. H. v. Löhneysen et al., *Physica B* **223 & 224**, 471 (1996)
11. A. Schröder et al., *Physica B* **199 & 200**, 47 (1994)
12. H. v. Löhneysen et al., *Phys. Rev. Lett.* **72**, 3262 (1994)
13. H. v. Löhneysen, *J. Phys.: Cond. Matt.* **8**, 9689 (1996) and refs. therein
14. O. Stockert et al., to be published
15. A. Schröder et al., to be published

16. Y. Noda et al., J. Phys. Soc. Japn. **54**, 4486 (1985); E. Gratz et al., J. Magn. Magn. Mater. **63** & **64**, 312 (1987)
17. D. Finsterbusch et al., Ann. Phys. **5**, 184 (1996)
18. A. Rosch et al., Phys. Rev. Lett. **79**, 159 (1997)
19. T. Sakihabara et al., J. Magn. Magn. Mat. **70**, 375 (1987)
20. T. Moriya and T. Takimoto, J. Phys. Soc. Japn. **64**, 960 (1995).
21. C. Paschke et al., J. Low Temp. Phys. **97**, 229 (1994)
22. See, e.g., G. A. Baker, *Quantitative Theory of Critical Phenomena*, (Academic Press, Boston, 1990)
23. U. Tutsch et al., unpublished results
24. Andrei, N., Phys. Lett. **87 A** 299 (1982).